Geophys. J. Int. (1998) 135, 1045–1059

The Oslo Rift: new palaeomagnetic and $^{40}Ar/^{39}Ar$ age constraints

Trond H. Torsvik,[1,2] Elizabeth A. Eide,[1] Joe G. Meert,[3] Mark A. Smethurst[1] and Harald J. Walderhaug[2]

[1] Geological Survey of Norway, PB 3006 Lade, N-7002 Trondheim, Norway. E-mail:trond.torsvik@ngu.no

[2] Institute of Solid Earth Physics, University of Bergen, Allegt. 41, N-5007 Bergen, Norway

[3] Department of Geography and Geology, Indiana State University, Terre Haute, IN 47809, USA

Accepted 1998 July 24. Received 1998 May 28; in original form 1998 January 29

SUMMARY

$^{40}Ar/^{39}Ar$ whole-rock and alkali feldspar ages demonstrate that dioritic to monzonitic dykes from Bøverbru and Lunner belong to the youngest recorded magmatic activity in the Oslo Rift region, southeast Norway. These dykes represent the terminal phase of rift and magmatic activity in the Oslo Graben, at the dawn of the Triassic (246–238 Ma).

The Bøverbru and Lunner dyke ages are statistically concordant. However, the palaeomagnetic signature of the Bøverbru dyke is complex, and directions from the margins and the interior of the dyke differ in polarity. Therefore, the new Early Triassic palaeomagnetic pole for Baltica (Eurasia) is exclusively based on the less complex Lunner dykes and contacts (palaeomagnetic pole: latitude = 52.9°N, longitude = 164.4°E, dp/dm = 4.5°/7.3°). The early Triassic palaeomagnetic pole [mean age: 243 ± 5 Ma (2s)] is slightly different from the Upper Carboniferous–Permian (294–274 Ma) and Kiaman-aged poles from the Oslo Rift.

Key words: dykes, geochronology, Oslo Rift, palaeomagnetism.

INTRODUCTION AND GEOLOGY

The Oslo Rift system and its associated tract of intrusive rocks are fundamental Permo-Carboniferous features in southern Norway (Ramberg 1976; Ramberg & Larsen 1978; Neuman 1994; Sundvoll & Larsen 1994; Olaussen et al. 1994) (Fig. 1). Palaeomagnetically analysed rocks from the Oslo Graben show a predominance of reverse polarities (Van Everdingen 1960; Douglass 1989), which comes as no surprise since the ca. 310–240 Ma (Sundvoll & Larsen 1990, 1994) magmatic activity in the region partially overlaps with the Kiaman Reverse Superchron (KRS) (ca. 311–262 Ma; Eide & Torsvik 1996 and references therein).

Magmatic activity in the Oslo Rift did persist after the KRS and, as part of an ongoing regional palaeomagnetic and isotopic dating program in SE Norway, we present a detailed account of palaeomagnetic and $^{40}Ar/^{39}Ar$ experiments from some of these younger, rift-related rocks. In the northern part of the Oslo Rift region we focus on dykes from the Bøverbru and Lunner areas (Fig. 1) and the Mjøsa Limestone rocks they intrude. The Upper Ordovician Mjøsa Limestone has been described by Bjørlykke (1983) and Opalinski & Harland (1981), but to our knowledge none of the dykes investigated at Bøverbru and Lunner (new 1995 road-cut) has been mentioned in the literature.

Following a Devonian–Early Carboniferous lacuna (subaerial exposure) for much of southern Norway, the rocks in the Oslo region experienced a continuous series of events related to the final amalgamation of Pangea. The climax of this Late Palaeozoic activity in the Oslo region includes N–S compression and related dextral transpression and transtension as Variscan tectonics advanced northwards in continental Europe. Dextral transtension led to the development of a purely extensional regime in the Oslo Rift system and the culmination of rifting and peak magmatic activity in the Oslo Graben (ca. 279 Ma; Olaussen et al. 1994; Heeremans et al. 1996). The latest Permian–Early Triassic period in the Oslo area has been described as the 'termination phase' of the evolution of the Oslo Rift system; this latest episode was associated with emplacement of small syenitic to granitic batholiths (Sundvoll & Larsen 1994; Olaussen et al. 1994). The two study areas (Fig. 1) are free from these young batholithic intrusions, and the only magmatic rocks previously described from this northern section of the Oslo Graben have been rhombporphyry (RP) rocks in the Lunner region (a dyke at Roa dated to 273 ± 7 Ma; Rb–Sr, Sundvoll & Larsen 1993), and a NNW–SSE chain of gabbroic necks dated to 266 ± 6 Ma (K/Ar, Neuman et al. 1985). The RP dykes are outliers of the massive RP lavas extruded in the southern–central Oslo Graben during the peak rifting phase (Olaussen et al. 1994).

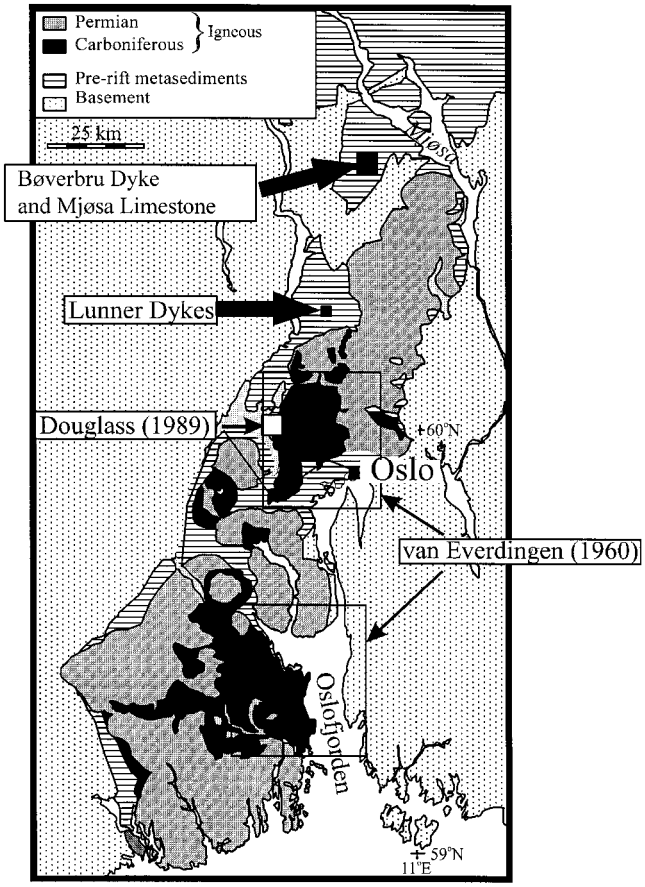

Figure 1. Geological sketch map of the Oslo Rift (SE Norway), showing sampling areas from this study and those of Douglass (1989) and van Everdingen (1960).

PALAEOMAGNETIC MEASUREMENTS

The natural remanent magnetization (NRM) was measured on a 2G Squid and a JR5A spinner magnetometer. Remanence stability was tested by progressive thermal (MMTD60), and to a minor extent alternating field (AF), demagnetization (2-axis tumbler). Characteristic remanence directions were determined using the least-squares regression analysis implemented in the SIAPD computer program (available at http://www.ngu.no/geophysics). Thermomagnetic analysis was performed on a horizontal translation balance.

Bøverbru dyke

The 1.3–1.4 m wide Bøverbru diorite dyke cuts perpendicular to E–W-striking, steeply dipping to overturned beds of the Upper Ordovician Mjøsa limestone. The limestone contacts with the dyke are baked in zones that extend 10–12 cm away from the contact; syn- or post-intrusion fluid influx along this contact is evident via mineralized veins and fractures and secondary alteration of the limestone. The chilled margins of the dyke are 12–15 cm wide, although the boundaries towardss the more crystalline dyke interior are diffuse.

Typical demagnetization behaviour for Bøverbru dyke and contact limestone samples is illustrated in Figs 2(a)–(d). High magnetic stability for baked limestone samples is reflected by almost univectorial demagnetization behaviour (Fig. 2b): reverse field directions with southerly or SSW declinations and steep negative inclinations characterize the baked limestone. Away from the baked zone, we identify a normal polarity, low unblocking remanence component (LB) ($<$150–250 °C, Fig. 2a). Curie temperatures between 570 and 580 °C and the unblocking temperature spectra suggest that magnetite is the prime remanence carrier for the host limestone.

The natural remanent intensity (NRM) and susceptibility data for the Mjøsa limestone surrounding the dyke average 2 mA m^{-1} and 95 (10^{-6} SI units). The baked limestone samples have higher NRM intensity, increasing towards the dyke contact (up to 40 mA m^{-1}; Fig. 2e). NRM and susceptibility values for dyke samples reach a maximum towards the centre, although we note a small minimum in the mid-section of the dyke. The demagnetization data from the Bøverbru dyke are remarkable due to the different directions of the margins and the interior of the dyke.

Table 1. Palaeomagnetic results from Bøverbru and Lunner dykes.

Site/Area	Pol	Dec°	Inc°	N	a_{95}	k	Comment
Bøverbru Quarry:							
B2 Bøverbru dyke	N	359.8	+70.3	46	5.6	14.9	HB Interior, LB margin
(130–140cm, 152/86)	R	198.3	−72.6	14	3.4	141.5	HB margin
B3 Contact Limestone (0–40 cm)	N	356.3	+49.5	6	11.7	33.8	LB
	R	188.5	−60.3	25	2.2	169.6	HB
B4 Limestone (0.72–4 meters)	N	354.8	+59.2	9	7.1	54.3	LB
(Transitional)	R	197.8	−40.1	11	6.7	47.7	HB
Lunner dykes (width, strike/dip):							
L1 (85 cm, 140/84)	R	199.1	−48.3	6	10.9	38.5	HB
Contact Limestone	R	197.7	−42.7	3	7.7	259.5	HB
L2 (350cm, 200/80)	R	205.2	−45.5	6	8.9	58.1	HB
Contact Limestone	R	202.2	−42.6	7	3.6	278.6	HB
L3 (120cm, 200/81)	R	200.3	−31.1	3	23.8	28.0	HB
Contact Limestone	R	202.9	−40.4	2	26.2	93.1	HB
L4 (67 & 153cm, 152/90)	R	176.2	−44.5	5	12.2	40.0	HB
Contact Limestone	R	191.3	−47.5	8	3.7	227.5	HB

Dec°/Inc°: mean declination/inclination; N: number of samples; a_{95}: 95 per cent confidence circle; k: precision parameter; HB: high unblocking component; LB: low unblocking component; Pol: magnetic polarity; N/R: normal/reverse polarity

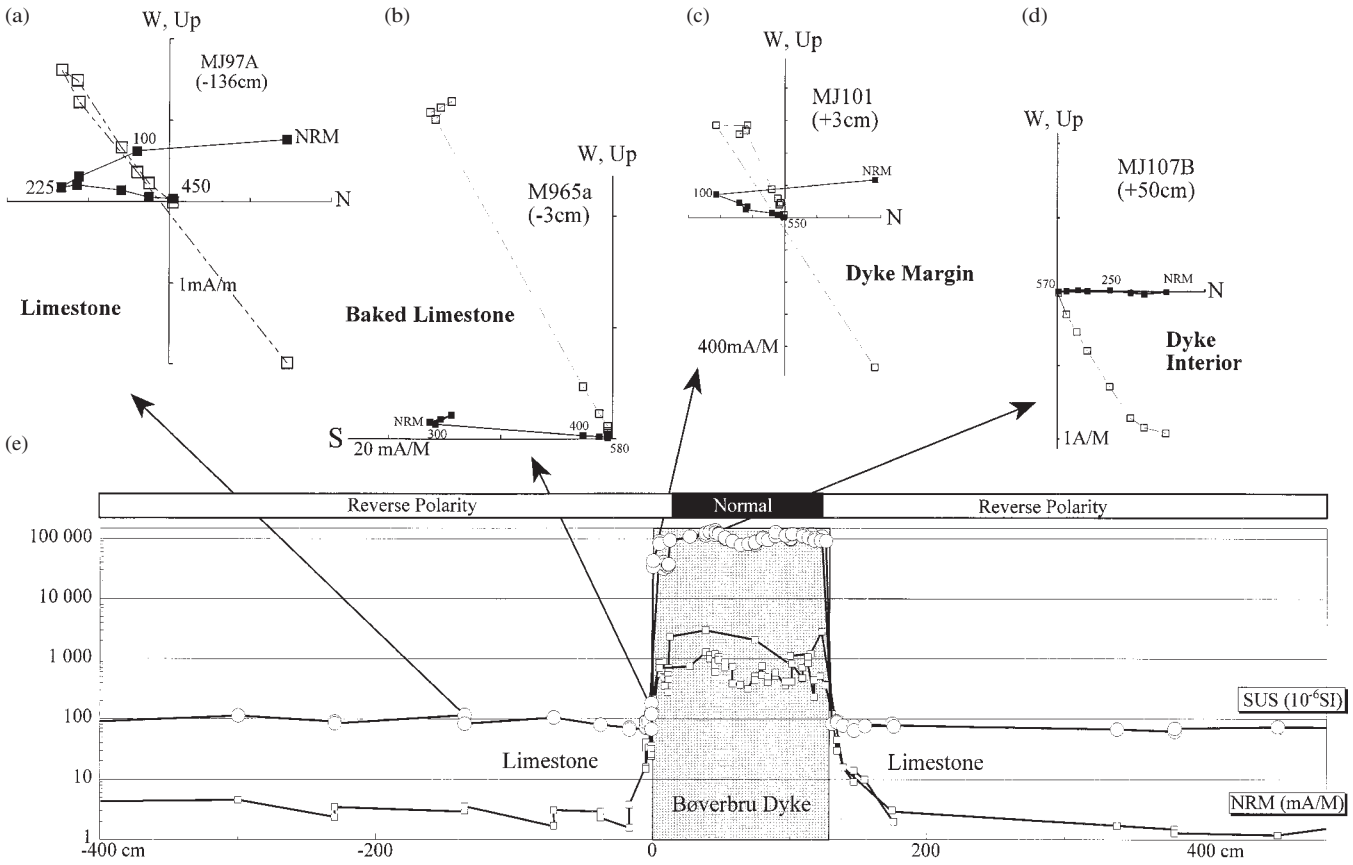

Figure 2. (a)–(d) Examples of thermal demagnetization from the Bøverbru dyke and the host Mjøsa Limestone. (e) NRM intensity and susceptibility variations through the Bøverbø dyke and host Mjøsa Limestone. The contact and dyke are sampled in two profiles. Magnetic polarity is based on high unblocking (HB) components. In the vector diagrams, open (closed) symbols denote points in the vertical (horizontal) plane.

(1) Fine-grained, chilled margin samples (< 12–15 cm wide zones) are characterized by reverse polarity high unblocking remanence components (HB) with steep negative inclinations and southerly declinations (Fig. 2c) that are similar to baked limestone directions (Fig. 2b). These data are distinct from the somewhat shallower directions observed in the non-baked Mjøsa limestone (Tables 1 and 2) and the 'transition limestone' about 72 centimetres away from the dyke contact (Fig. 2a), and thus indicate a positive contact test. Samples from the dyke margins show a tight (quenched) directional clustering (HB, reverse polarity component) which is comparable to that of contact limestone samples (Figs 3a and b).

(2) In contrast, the interior parts of the dyke are exclusively characterized by normal polarity, HB components with northerly declinations (Figs 2d and 3a). This normal polarity component is commonly identified as a LB component in marginal dyke samples (Figs 2c and 3a).

Maximum thermal unblocking temperatures in the 550–580 °C range suggest titanium-poor titanomagnetite (TM) or nearly pure magnetite as the bulk remanence carrier for both normal and reverse dyke sample directions. The median destructive field ($M_{1/2}$) is typically around 35 mT, with IRM saturation at around 300–350 mT for marginal samples. Lower $M_{1/2}$ ($\approx$10mT) and IRM saturation fields (200–250 mT) for interior samples reflect the coarser grain size in this part of the dyke. Thermomagnetic analyses reveal distinct magneto-mineralogical differences between marginal and interior parts of the dyke (Fig. 4).

(1) Marginal dyke samples (reverse polarity) are characterized by a combination of magnetite and maghemite. During heating, saturation magnetization first increases and shows a kink at 150–170 °C (cooling at 200–300 °C produces a reversible phase), followed by inversion of maghemite to a weaker magnetic phase at $\approx$350 °C, and finally Curie temperatures at around 580 °C (Fig. 4a). The kink at 150–170 °C (Fig. 4a—marginal samples) is a typical low-temperature TM (maghemitization) phenomenon (Ade-Hall et al. 1971).

(2) The interior parts of the dyke (normal polarity) show single Curie temperatures at $\approx$580 °C (Fig. 4b), indicative of titanium-poor TM. Reduced saturation magnetization after cooling indicates some oxidation.

Opaque mineralogy at the centre of the dyke (Fig. 4d) is dominated by TM grains of up to 200 mm in size. Grains show extensive evidence of low-temperature alteration such as contraction cracks (maghemitization) and granulation. Minor amounts of pyrite are present as small inclusions in some of the grains. No high-temperature exsolution features are observed, attesting to the fairly rapid cooling of the dyke. Near dyke margins (Fig. 4c), the maximum grain size decreases to $\approx$100 mm, and numerous smaller grains (d < 10 mm) appear. In addition to the same alteration features as observed in the

Table 2. Site-mean directions from the Upper Ordovician (Caradoc) Mjøsa Limestone.

Area/ Site	Bedding Strike/Dip	Pol	In-situ Dec°	Inc°	N	a_{95}	k	100% unfolded Dec°	Inc°	Comment
Bøverbru Quarry (60.7°N, 10.7°E):										
B1	090/93	N	026.1	+58.2	6	5.0	178.7	165.1	+25.3	LB
		R	196.1	−39.3	8	3.9	206.3	342.3	−45.2	HB
Moen Quarry (60.7°N, 10.7°E):										
M1	081/75	N	022.4	+65.7	10	5.9	67.2	155.8	+35.1	LB
		R	196.8	−36.4	9	5.9	76.6	308.7	−58.6	HB
M2	106/76	N	340.2	+66.0	5	10.5	54.4	212.4	+32.8	LB
		R	203.3	−34.9	5	11.0	49.8	359.8	−68.1	HB
M3	114/77	N	342.2	+68.8	4	10.4	79.2	219.9	+28.2	LB
		R	194.2	−32.2	7	7.1	72.7	047.5	−68.8	HB
M4	110/77	N	024.4	+60.1	4	13.5	47.0	197.0	+42.8	LB
		R	199.9	−33.9	7	2.8	476.8	020.2	−69.1	HB
M5	113/60	N	347.0	+69.5	3	6.0	427.7	220.1	45.5	LB
		R	207.2	−29.9	6	11.5	34.9	292.5	−86.4	HB
Mean L B										
B1, B3-B4*, M1-M5		N	002.9	63.3	8#	7.6	54.0	188.7	36.6	LB
M1-M5						15.8	13.2	(unfolded parameters)§		
Mean HB										
B1,B4*, M1-M5		R	199.4	−35.3	7#	3.9	237.3	015.4	−72.7	HB
						23.1	7.8	(unfolded parameters)§		

* from Table 1. N: samples/sites#; § Statistically negative fold test at the 95 per cent confidence level. See Table 1 for further details.

dyke interior, red staining around grain margins is evident under polarized light, suggesting the formation of secondary haematite.

Lunner dykes (four sites)

Dyke trends and nearly vertical dips at Lunner sites 4 and 1 (L4 and L1) are comparable with the structural orientation of the Bøverbu dyke, while dykes at Lunner sites 2 and 3 (L2 and L3) strike 200° (Table 1). Lunner dykes and the associated contact limestone show comparable HB directions with SSW declinations and negative inclinations (Figs 3c–d). Limestone samples are essentially single-component (Fig. 5a), while dyke samples from Lunner dykes 1 and 4 (Figs 3c and 5b) show minor, but often poorly defined, LB components. Maximum unblocking temperatures are 550–565 °C for both dyke and contact limestone. LB components are directionally smeared (Fig. 3c); hence we have not calculated a mean direction for LB components from the Lunner dykes.

Mjøsa Limestone (six sites)

The regional magnetic signature of the Upper Ordovician (Caradoc) Mjøsa limestone was tested for six sites in the Bøverbru area (Table 2, Fig. 1). The Mjøsa Limestone in the study area comprises a bioturbated limestone, with some dolomitization. All samples are dominated by steep positive LB components with northerly declinations and HB components with SSW declination and negative inclination (Fig. 6a). Directional stability for the HB component was never observed above 500 °C (Fig. 6b), at which point remanence intensity dropped below the instrument sensitivity levels. Both LB and HB components fail a fold test (Table 2), and both components are therefore of secondary and post-fold origin.

40AR/39AR EXPERIMENTS

Prior to 40Ar/39Ar furnace step-heating, clean Bøverbru ('M') and Lunner ('LU') whole rock (M103, M106, LU1 and LU4) and plagioclase (LU1A) fractions (180–250 m) were packed in Sn-foil and irradiated at the Siloe reactor in Grenoble, France. We used the 40Ar/39Ar analytical facility at the Universite Blaise Pascal et Centre National de la Recherche Scientifique, Clermont-Ferrand, France, with analytical protocol and irradiation parameters similar to those used by Arnaud et al. (1993). Samples were step-heated using a radio-frequency furnace with temperature calibration (10 °C) by an optical pyrometer. Each 25 min heating step was gettered for 5 min prior to inlet, and samples were degassed at 400 °C for 25 min before the analysis. Mineral compositional data are reported in Table 3; 40Ar/39Ar data are reported in Tables 4 and 5 and Figs 7 and 8. The two Bøverbru samples were irradiated separately from the three Lunner samples (on different days); thus, we incorporate the inter-laboratory uncertainty in J-value (2 per cent) when making inter-locality age comparisons (Table 5), but we do not include the J-value error when tabulating the Bøverbru or Lunner data alone (Table 4). We cite uncertainties at the 1s level. Plateaus are defined as comprising three or more contiguous steps that overlap at the 95 per cent confidence level and together constitute more than 50 per cent of the total experimental gas. Individual steps were 'weighted' by both length (gas volume) and individual age uncertainty (IAAA software, integrated analysis of argon–argon data, is available at http://www.ngu.no/geophysics).

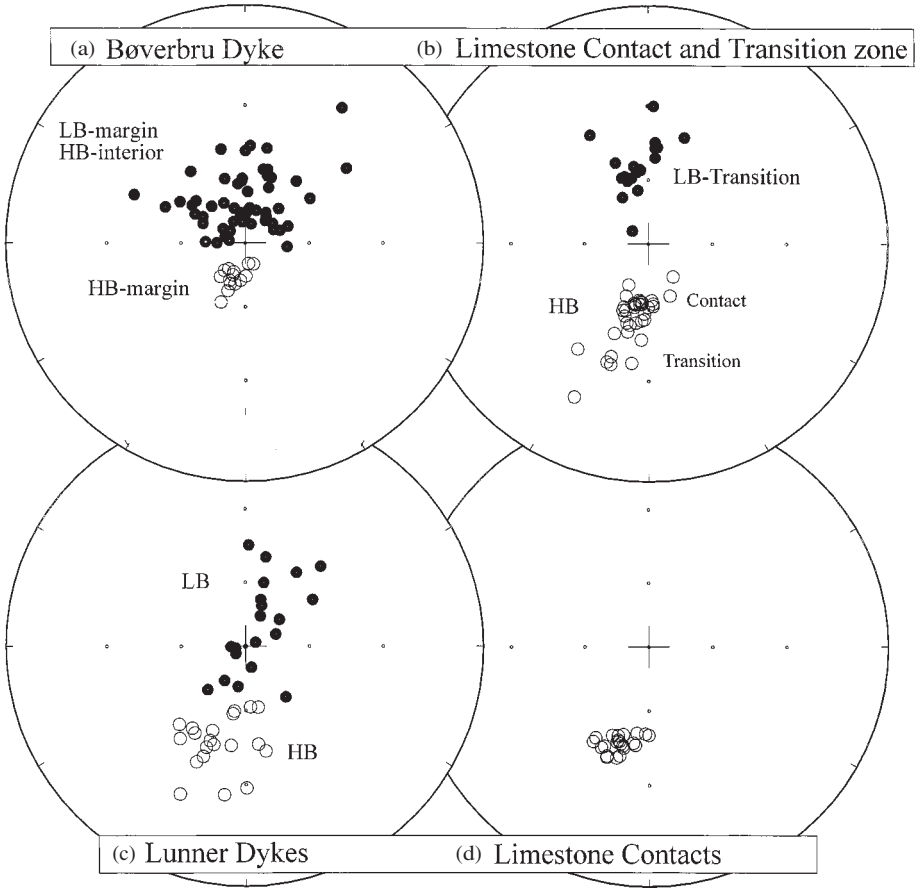

Figure 3. Characteristic remanence components from Bøverbru dyke (a) and host limestone contact and transition zone (b). (c) and (d) show remanence components from Lunner dykes and limestone contacts. In the stereoplots (a,c), open (closed) symbols denote negative (positive) inclinations. HB/LB: high/low unblocking remanence components.

Monitor minerals were the Fish Canyon Tuff feldspar (27.4 Ma, Cebula et al. 1986) and the Caplongue hornblende (344.5 Ma, Maluski 1989).

Bøverbu dyke

Two cores were analysed from Bøverbru. Sample M103 was drilled from the middle of the reverse polarity, chilled dyke margin (13 cm from west margin), and sample M106 was from the coarser-grained and normal polarity dyke centre (88 cm from west margin).

The chilled margin is aphanitic to slightly porphyritic with albitic feldspar phenocrysts in a groundmass of greenish-grey glass and feldspar microlites. Groundmass feldspar is fuzzy and occluded and the larger phenocrysts are often replaced by calcite and sericite. Minor chlorite alteration is evident. The

Table 3. Representative electron microprobe analyses of feldspar (fsp) and clinopyroxe (cpx) from Bøverbru and Lunner (LU) dykes. R: analysis of grain rim; C: analysis of grain core. Feldspars are albitic, with slightly higher K_2O in grain cores than rims; clinopyroxene in Bøverbru is augitic.

Oxide	Bøverbru fsp (R)	Bøverbru fsp (C)	LU4 fsp (C)	LU4 fsp (R)	Oxide	Bøverbru cpx
SiO_2	66.89	66.23	66.34	67.38	SiO_2	47.47
Al_2O_3	20.97	21.65	20.72	20.27	TiO_2	1.88
FeO	0.26	0.4	0.95	0.75	Al_2O_3	7.78
CaO	0.44	0.58	1.47	0.94	MgO	12.79
Na_2O	10.85	10.16	10.55	11.02	FeO	7.54
K_2O	0.7	1.27	0.28	0.16	MnO	0.11
BaO	0	0	0.03	0.03	CaO	21.49
Total	100.11	100.29	100.34	100.55	Na_2O	0.63
					K_2O	0.00
					Cr_2O_3	0.23
					NiO	0.00
					Total	99.92

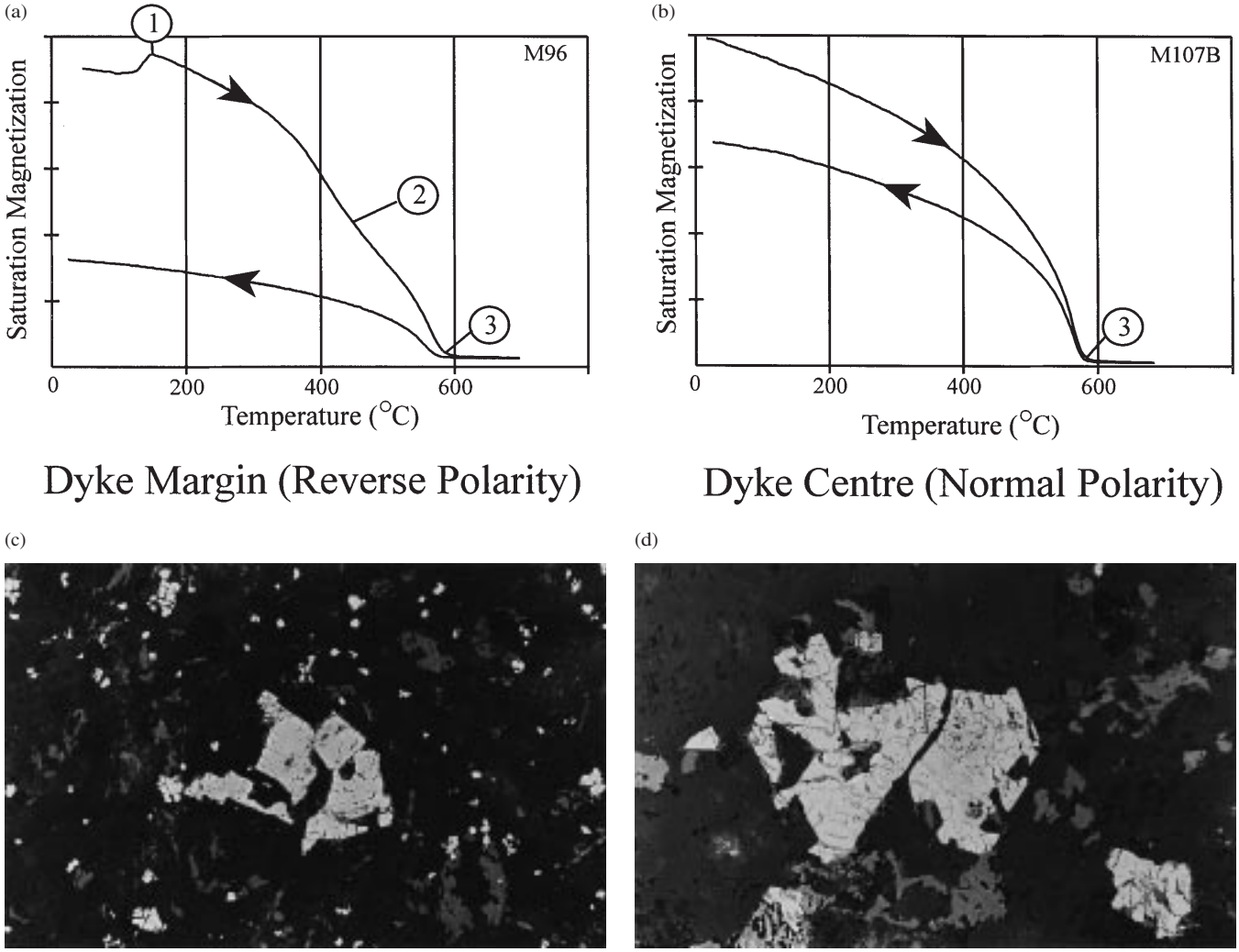

Figure 4. Thermomagnetic analysis of samples from the Bøverbru dyke margin (a) and centre (b). (1) Kink at 150–180 °C (irreversible creation of a magnetic phase with higher saturation magnetization); (2) inversion of maghemite to a weaker (haematite) magnetic phase at T > 350 °C; (3) magnetite $T_c \approx 580$ °C. (c) Reflected-light micrograph from margin of Bøverbru dyke (frame width = 330 mm). Note the presence of numerous small TM grains as well as larger grains with distinct low-temperature alteration features. (d) Reflected-light micrograph for the centre of Bøverbru dyke showing TM grains with low-temperature alteration features (frame width = 330 mm).

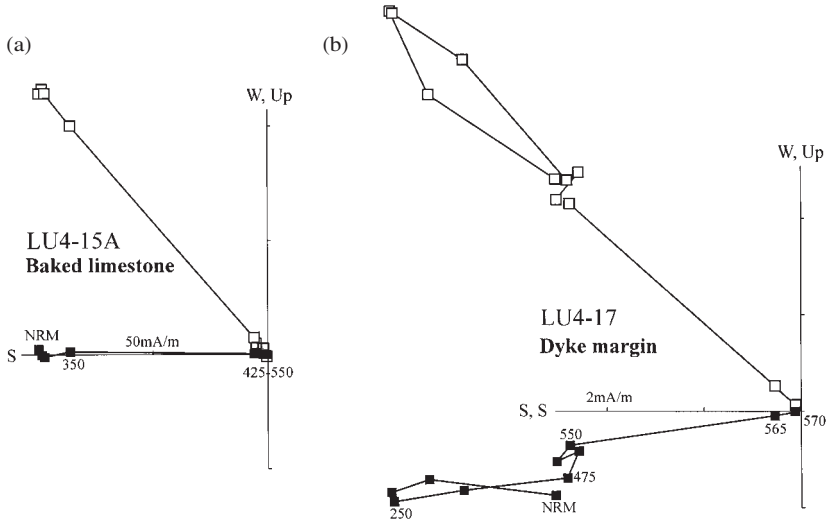

Figure 5. Examples of thermal demagnetization from Lunner dyke 4: baked limestone (a) and dyke margin (b).

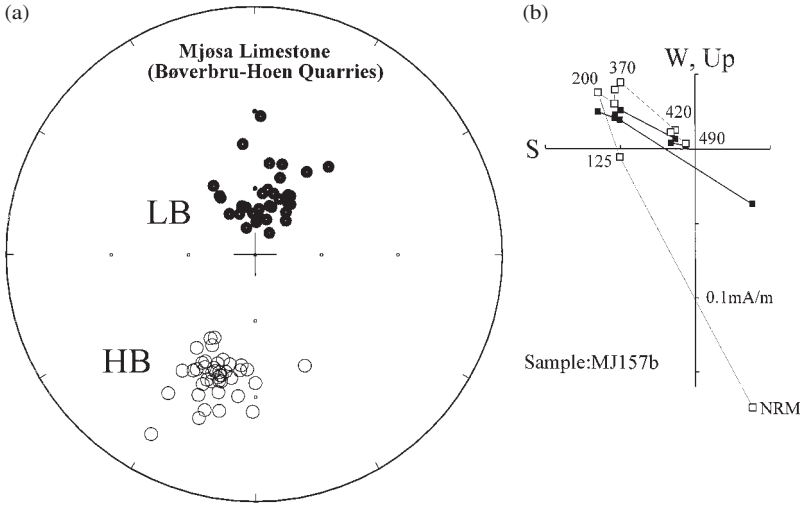

Figure 6. Characteristic remanence components (a) and example of thermal demagnetization (b) for the Mjøsa Limestone.

coarse-grained dyke centre has a porphyritic, intersertal texture with coarse-grained clinopyroxene phenocrysts (augite, Table 3), coarse albitic feldspar (Table 3), minor amphibole and a groundmass of fine-grained plagioclase laths, amphibole needles, oxides, and minor interstitial glass. As with the other zones of the dyke, feldspars are slightly occluded and replaced by sericite and calcite. Chlorite occurs in numerous cracks in clinopyroxene and calcite replaces amphibole.

$^{40}Ar/^{39}Ar$ data from sample M103 (chilled margin) yield total fusion (TFA) and isochron ages (242.0 ± 5.3 Ma, 237.9 ± 8.1 Ma, respectively) within analytical uncertainty of one another, and nearly within uncertainty of the weighted mean plateau age (WMPA) (245.5 ± 4.6 Ma) (Fig. 7; Tables 4 and 5). The six-step release spectrum is characterized by four broadly concordant temperature steps that range in age from 240 to 252 Ma and represent 91.6 per cent of the cumulative ^{39}Ar released. The large gas volume and slightly higher age of the fifth step in the plateau is responsible for the lack of age-overlap between the WMPA and the isochron age. The Ar-release pattern for M106 (dyke centre) comprises eight steps, three of which are concordant at 242.5 ± 4.6 Ma in the middle temperature range (38.4 per cent of cumulative ^{39}Ar); these steps are preceded by two low-age concordant steps and succeeded by a stair-step increase in apparent ages until fusion (Fig. 7, Tables 4 and 5).

The K/Ca and $^{38}Ar_{Cl}/^{39}Ar_{K}$ plots (Fig. 7) indicate progressive Ar release from different mineral phases in the whole rocks. The first steps in both spectra, with the lowest apparent ages, are consistent with degassing from slightly altered, fine-grained, low-K groundmass that has undergone some Ar loss. In the case of M106, these low ages are also Cl-correlated and may indicate a contribution from the chlorite alteration on the pyroxenes in the sample. The central portions of each spectra, comprising broadly concordant steps (in M106) or plateau steps (in M103), yield gas from relatively high-K phases with minimal Cl-content which we attribute to degassing of groundmass, fine-grained feldspar and, later, feldspar phenocrysts over furnace temperatures of ≈ 900–$1100\,^{\circ}C$. The final steps indicate exhaustion of K-bearing phases and increased release from Cl- and Ca-correlated Ar components. In the case of the chilled margin (M103), the latter effect is restricted to a very low-volume final (fusion) step comprising mostly air, while M106 shows definite effects of degassing from Ca- and Cl-rich amphibole and clinopyroxene phenocrysts (Fig. 7).

Lunner dykes

The Lunner 1 sample, LU1, is a pale grey, cryptocrystalline to slightly porphyritic rock with phenocrysts of fine- to medium-grained alkali feldspar, oxides, rare biotite, and some groundmass glass. Coarse feldspar laths are somewhat mottled due to replacement by sericite(?), but appeared fairly fresh and pink to pink-translucent when separated. Lunner sample LU4 has a similar appearance to the Bøverbru dyke, with grey-green colour and feldspar phenocrysts, but it lacks clinopyroxene. The rock is cryptocrystalline with some large albitic feldspar phenocrysts in a matrix of equigranular feldspar, oxides, minor glass and chlorite (see Table 3).

The $^{40}Ar/^{39}Ar$ release spectrum for LU1 (Fig. 8) defines a plateau of 237.2 ± 4.4 Ma (62.3 per cent of ^{39}Ar gas). The plateau is preceded by two initial, low-temperature, low-age steps, and succeeded by three, rising, apparent ages that reach a maximum of 267 Ma at fusion. The steps in the plateau itself exhibit a slight and consistent increase with increasing temperature (Fig. 8a). On an isochron, the plateau steps cluster as a very radiogenic group of points with poor correlation to an ordinate intercept of 241.4 ± 8.4 Ma and an abscissa intercept ($^{40}Ar/^{36}Ar$ ratio) of 235 ± 60 (atmospheric value $= 295.5$). The alkali feldspar separate (LU1A, from rock LU1) defines a plateau of 246.2 ± 4.6 Ma for 58.6 per cent of ^{39}Ar released (Fig. 8b). Two initial, low-age, low-volume steps are Cl-correlated, while the central and final portions of the pattern indicate Ar gas derived from the K-rich feldspar.

The high, but very variable K/Ca ratios for the 'rising' plateau portion of whole-rock analysis LU1 suggest Ar was released from at least two K-bearing phases: a very high-K phase (higher temperatures in the furnace heating experiment) and a phase with slightly less K (middle-temperature portion of the plateau) (compare, for example, to K/Ca ratios for Bøverbru and LU4, Figs 7 and 8c). The release of Ar from two different high-K reservoirs in LU1 corresponds to the presence of both alkali feldspar and biotite in the rock, and probably documents the different closure temperatures of these minerals over the ≈ 10 Myr age range represented in the

Table 4. 40Ar/39Ar furnace step-heating data.

(a) Bøverbru Dyke, sample M103 Whole Rock (J = 0.0067, weight = 12.85 mg): 13 cm from west contact (chilled margin).

Temp °C	40Ar/39Ar	38Ar/39Ar	37Ar/39Ar	36Ar/39Ar (10^{-3})	39Ar (10^{-14} mol)	F39Ar released	%40Ar*	40Ar*/39Ar	Age (Ma)	±1s Ma
700	21.008	0.054	0.948	23.070	1.00	7.95	66.86	14.44	166.62	4.24
800	25.019	0.052	13.688	19.345	0.87	14.82	81.77	21.29	240.54	4.27
900	23.662	0.047	0.368	7.002	0.83	21.48	88.99	21.68	244.70	4.22
1000	23.839	0.062	0.216	10.000	3.39	48.56	87.31	20.97	237.17	3.80
1100	28.023	0.123	0.635	19.783	6.38	99.53	79.53	22.37	252.00	5.22
1150	82.702	0.000	0.000	196.743	0.06	100.00	2.52	25.65	286.07	16.49

(b) Bøverbru Dyke, sample M106 Whole Rock (J = 0.00676, weight = 13.0 mg): 88 cm from west contact (centre).

Temp °C	40Ar/39Ar	38Ar/39Ar	37Ar/39Ar	36Ar/39Ar (10^{-3})	39Ar (10^{-14} mol)	F39Ar released	%40Ar*	40Ar*/39Ar	Age (Ma)	±1s Ma
700	30.209	0.196	2.877	37.844	0.12	4.95	62.92	19.57	224.19	5.46
800	22.688	0.071	14.078	16.814	0.07	7.94	79.87	19.62	224.66	5.54
900	23.934	0.055	4.163	7.964	0.11	12.34	88.24	22.15	251.71	6.14
1000	24.414	0.047	0.304	11.023	0.36	27.07	85.74	21.22	241.84	5.54
1050	22.668	0.060	0.379	5.341	0.47	46.42	91.29	21.13	240.89	5.13
1100	24.595	0.116	0.910	5.731	0.72	75.75	91.78	23.02	260.92	5.55
1200	29.330	0.180	3.329	10.575	0.57	99.11	87.79	26.70	299.33	6.00
1400	120.499	0.249	70.931	352.760	0.02	100.00	15.92	28.38	316.66	48.3

(c) Lunner Dyke, sample LU1A Alkali feldspar (J = 0.016980, weight = 5.0 mg).

Temp °C	40Ar/39Ar	38Ar/39Ar	37Ar/39Ar	36Ar/39Ar (10^{-3})	39Ar (10^{-14} mol)	F39Ar released	%40Ar*	40Ar*/39Ar	Age (Ma)	±1s Ma
600	30.234	0.058	0.068	85.145	0.520	4.15	18.3	5.54	162.29	13.15
700	37.762	0.042	0.110	102.927	0.527	8.36	21.0	7.92	227.66	9.61
750	10.260	0.019	0.015	5.327	2.530	28.55	84.9	8.71	248.86	5.39
800	10.157	0.020	0.016	5.181	0.890	35.66	85.2	8.65	247.24	5.79
850	9.786	0.019	0.009	4.636	1.241	45.57	86.2	8.44	241.53	5.62
900	9.700	0.019	0.007	4.400	1.361	56.43	86.8	8.42	241.05	5.24
950	9.923	0.019	0.012	4.429	0.797	62.79	87.0	8.63	246.80	5.58
1000	10.16	0.019	0.010	4.594	0.525	66.98	86.8	8.82	251.86	5.64
1050	9.388	0.019	0.009	3.822	0.533	71.23	88.1	8.28	237.20	4.48
1100	9.423	0.019	0.007	4.012	0.539	75.53	87.6	8.25	236.65	4.49
1200	9.704	0.019	0.006	4.466	1.702	89.12	86.6	8.40	240.63	4.52
1400	10.601	0.019	0.067	5.088	1.363	100.00	86.1	9.13	259.98	6.02

(d) Lunner Dyke 1, sample LU1 Whole Rock (J = 0.01670, weight = 5.0 mg).

Temp °C	40Ar/39Ar	38Ar/39Ar	37Ar/39Ar	36Ar/39Ar (10^{-3})	39Ar (10^{-14} mol)	F39Ar released	%40Ar*	40Ar*/39Ar	Age (Ma)	±1s Ma
600	7.132	0.019	0.144	6.187	9.644	14.57	74.9	5.35	156.71	3.48
700	10.138	0.020	0.058	11.327	10.025	29.7	67.6	6.85	198.52	4.67
750	9.481	0.019	0.021	4.762	8.012	41.79	85.4	8.10	232.26	4.89
800	8.776	0.019	0.016	2.353	3.775	47.48	92.2	8.09	232.08	4.87
850	8.823	0.018	0.014	2.368	3.176	52.28	92.2	8.13	233.21	5.00
900	9.019	0.019	0.016	2.876	2.748	56.42	90.7	8.18	234.54	4.99
950	8.980	0.018	0.014	2.773	3.581	61.83	91.0	8.17	234.29	4.89
1000	9.069	0.018	0.01	2.788	5.238	69.73	91.0	8.26	236.54	4.89
1050	9.260	0.019	0.01	3.261	6.214	79.10	89.7	8.31	237.99	5.09
1100	9.225	0.018	0.011	2.683	5.039	86.71	91.5	8.44	241.55	5.32
1150	9.159	0.018	0.014	1.988	3.496	91.98	93.7	8.58	245.20	5.42
1200	9.604	0.019	0.023	3.185	1.428	94.14	90.3	8.68	247.84	5.33
1400	10.213	0.018	0.03	2.762	3.884	100.00	92.1	9.41	267.29	5.51

Table 4. (Continued.)
(e) Lunner Dyke 4, sample LU4 Whole Rock (J = 0.016970, weight = 5.0 mg).

Temp °C	40Ar/39Ar	38Ar/39Ar	37Ar/39Ar	36Ar/39Ar (10⁻3)	39Ar (10⁻14 mol)	F39Ar released	%40Ar*	40Ar*/39Ar	Age (Ma)	±1s Ma
700	18.451	0.026	2.789	38.221	3.913	11.04	40.9	7.72	221.98	6.22
750	12.916	0.022	0.324	16.767	1.098	14.07	62.5	8.09	232.07	5.52
800	11.903	0.022	0.351	12.773	0.948	16.69	69	8.24	236.09	5.11
850	12.581	0.022	0.341	15.067	1.19	19.98	65.4	8.25	236.39	5.36
900	11.788	0.021	0.355	12.392	2.179	26.01	69.7	8.24	235.99	5.66
950	9.939	0.02	0.354	5.77	3.815	36.56	83.3	8.31	237.91	5.27
1000	9.342	0.019	0.386	3.867	4.213	48.22	88.2	8.27	236.8	5.02
1050	9.551	0.02	0.475	4.622	6.935	67.42	86.2	8.27	236.86	4.89
1100	10.317	0.02	0.914	6.746	3.425	76.93	81.6	8.48	242.47	5.03
1150	10.465	0.021	0.86	6.437	2.593	84.13	82.6	8.71	248.66	5.23
1200	12.825	0.021	0.86	9.234	0.587	85.76	79.5	10.27	289.79	6.36
1300	11.961	0.021	0.97	8.467	1.987	91.28	79.9	9.64	273.27	5.93
1400	13.194	0.021	0.794	10.908	3.14	100	76.4	10.14	286.47	6.96

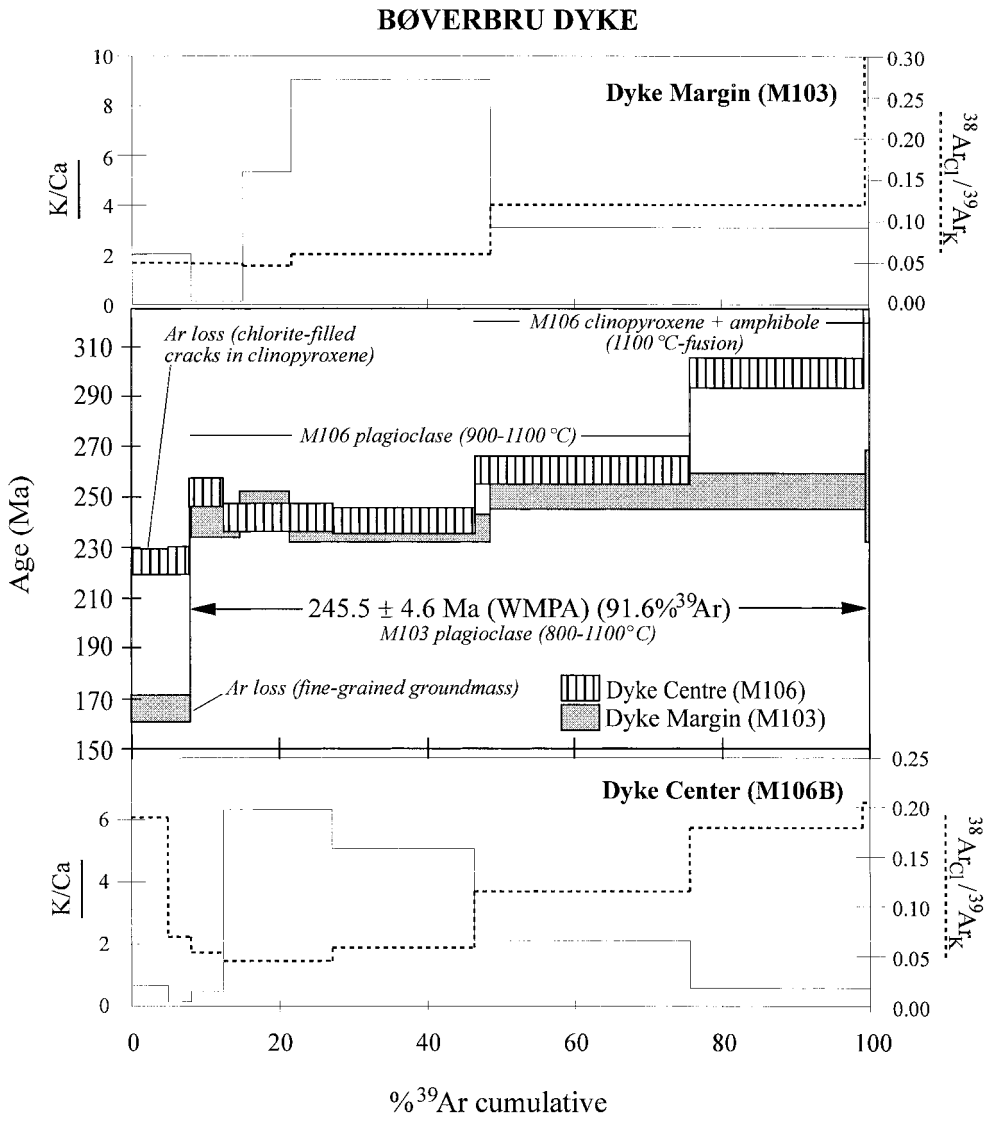

Figure 7. 40Ar/39Ar release spectra and K/Ca and Cl/K ratios for two whole-rock samples from the Bøverbru dyke. Sample M103 derives from the dyke margin and M106B from the coarse-grained dyke centre. The release spectrum for M103 yields a plateau age of 245.5 ± 4.6 Ma. Both spectra and their elemental ratios demonstrate the release of Ar gas from different phases in the whole rocks: plagioclase dominates the Ar-release pattern for both rocks, but the spectrum for M106b is complicated by the presence of excess Ar in coarse-grained amphiboles and clinopyroxenes.

Table 5. $^{40}Ar/^{39}Ar$ isotopic ages (1s including error in J).

Dyke	Sample	Mineral	Total Fusion Age ± 1s	Isochron Analysis N	MSWD	$^{40}Ar/^{36}Ar$ Intercept ± 1s	Age ± 1s	Age Spectrum N	^{39}Ar(%)	Age ± 1s	Utilised Age ± 1s
Bøverbru	M103	wr	242.0 ± 5.3	4	2.0	350 ± 53	237.9 ± 8.1	4	91.6	245.5 ± 4.6	245.5 ± 4.6
Bøverbru	M106	wr	265.6 ± 5.1	—	—	—		(3	38.4	242.5 ± 4.6)	
Lunner 1	Lunn1	wr	221.2 ± 4.2	10	5.48	235 ± 60	241.4 ± 8.4	9	62.3	237.2 ± 4.4	
Lunner 1	Lunn1a	fsp	241.8 ± 4.6	12	16.29	282 ± 11	240.8 ± 4.8	6	58.6	246.2 ± 4.6	246.2 ± 4.6
Lunner4	Lunn4	wr	243.7 ± 4.6	7	0.23	282 ± 8	238.2 ± 4.6	7	65.9	238.3 ± 4.5	238.3 ± 4.5
										Weighted Mean	243.3 ± 2.6

Table 6. Overview and interpretation of selected palaeomagnetic data from the Oslo Rift area.

Code*	Formation	Location Lat.	Long.	Dec°	Inc°	a_{95}	N	VGP Lat.	Long.	dp/dm	Age (±2s) or Comment
Primary data: Oslo Rift magmatic rocks:											
LU	Lunner dykes and contacts	60.3	10.5	197.1	−43.2	5.9	8	52.9	164.4	4.5/7.3	243 ± 5 Ma (Tables 1 & 5)
RL	Ringerike Lavas (B1-RP7-RP10) (Ages: 276 ± 6, 281 ± 6 & 291 ± 8)	60.0	10.25	204.0	−33.0	13.4	3	44.6	157.4	8.6/15.2	281 ± 4 Ma Rb-Sr (tilt corrected)
OGL	Oslo Graben Lavas (Ages: 274 ± 3, 276 ± 6, 277 ± 3, 278 ± 5, 278 ± 12, 278 ± 8, 279 ± 9, 280 ± 7, 281 ± 6, 281 ± 4, 284 ± 7, 288 ± 9, 288 ± 7, 290 ± 4, 291 ± 8, 291 ± 18, 292 ± 20 & 294 ± 6)	59.5	10.5	204.0	−36.0	1.5	27	47.0	157.0	1.0/1.7	281 ± 2 Ma Rb-Sr (tilt corrected)
Secondary data:											
Permian overprints related to main Oslo Rift magmatic pulse (code RL and OGL)											
MS-1	Mjøsa Limestone	60.5	10.7	199.4	−35.3	3.9	7	46.7	163.5	2.6/4.5	In-situ HB data (Table 2)
RS	Ringerike Sandstone	60.0	10.25	207.0	−36.0	2.9	19	45.6	152.7	2.0/3.4	
Jurassic-or-younger overprint related to thermo-viscous exhumation											
MS-2	Mjøsa Limestone	60.5	10.7	002.9	+63.3	7.6	8	74.2	183.1	9.5/12.0	In-situ LB data (Table 2)

* see Fig. 10; Lat./Long.: latitude/longitude; VGP: virtual palaeomagnetic pole; dp/dm: semi-axes of the cone of 95 per cent confidence about the pole. Ages for Ringerike and Oslo Graben lavas listed in Torsvik & Eide (1998). See Table 1 for further details.

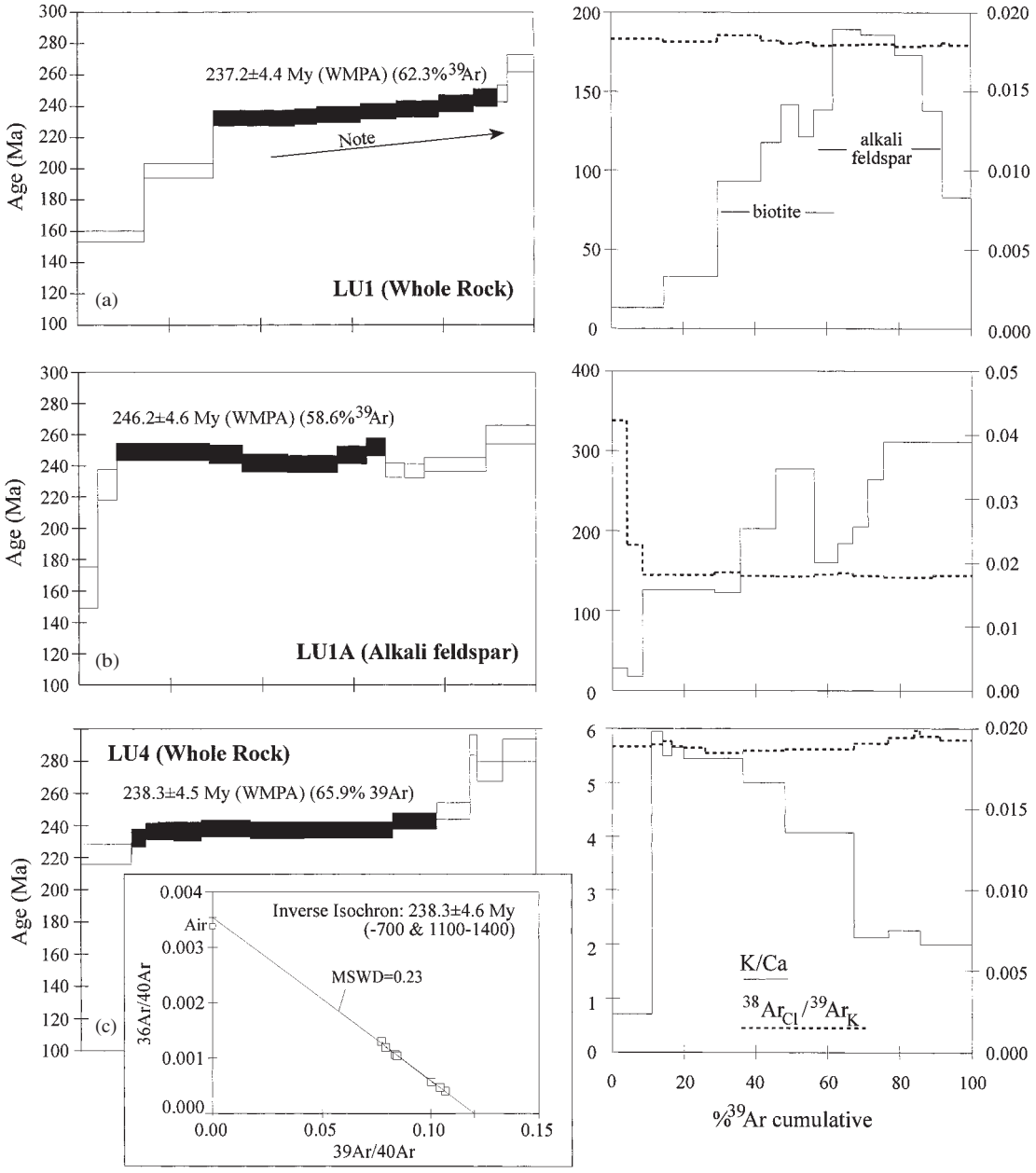

Figure 8. (a) Whole-rock 40Ar/39Ar release spectrum and element ratios for Lunner dyke LU1. The data define a statistically valid plateau age of 237.2 ± 4.4 Ma, but we note the slight but progressive rise in the steps with increasing temperature. The elemental ratios reveal that this results from degassing of two high-K phases during the experiment: biotite at slightly lower temperatures and K-feldspar at higher temperatures. This phenomenon is revealed in the spectrum in (b), a pure alkali feldspar separate from the same rock which yields a plateau age of 246.2 ± 4.6 Ma. (c) Whole-rock release spectrum and elemental ratios for Lunner dyke LU4. This sample contained only alkali feldspar as a high-K phase and yields both a plateau and isochron within analytical uncertainty (238.3 Ma). Portions of the spectra used to calculate cited plateau ages are in black.

plateau. The feldspar separate, LU1A, confirms the 'mixed' age of the whole-rock analysis, as well as the fact that the feldspar is the more retentive phase (i.e. releases its gas at higher temperatures) of the two in the rock.

Sample LU4 yielded a plateau age of 238.3 ± 4.5 Ma for 65.9 per cent of 39Ar gas released, and is similar within uncertainty to LU1 (Fig. 8). The 238.2 ± 4.6 Ma isochron age (also excluding the first and final four temperature steps) is indistinguishable from the plateau age, is well-correlated (MSWD = 0.23), and yields a 40Ar/36Ar value of 282 ± 8. Albitic feldspar is the dominant K-bearing phase in LU4, corresponding to Ar gas release during analysis at temperatures between 750 and 1000 °C. The excluded, lowermost temperature step is a product of degassing weakly bound Ar gas at grain surfaces. The excluded high-temperature steps in LU4 represent exhaustion of the feldspar gas and commencement of degassing from a different, high-Ca phase that we presume to be altered glassy groundmass.

INTERPRETATION AND DISCUSSION

Bøverbru and Lunner dykes

We consider the plateau age of 245.5 ± 4.6 Ma (sample M103) to date the crystallization age of the Bøverbru dyke. The age of 242.5 ± 4.6 Ma for the plagioclase-generated portion of M106 (dyke centre) is within uncertainty of the WMPA for M103 and should be expected, since this single dyke obviously cooled quickly. We nonetheless discount the reliability of the data from the M106 (dyke centre) sample because the majority of the gas release was governed by the effects of excess-Ar-containing components (pyroxene and amphibole). We interpret the plateau ages of 246.2 ± 4.6 Ma (LU1A, alkali feldspar) and 238.3 ± 4.5 Ma (LU4, whole rock) to represent the time of crystallization of the Lunner dykes. Despite differences in chemistry (and hence mineral compositions), the Lunner ages and the Bøverbru M103 age are concordant at the 95 per cent confidence level, and we cite a weighted mean age of 243.3 ± 2.6 Ma (i.e. early Triassic) for their crystallization to simplify subsequent discussion (see Table 5).

The mean palaeomagnetic directions from the Lunner dykes and their high-stability contact limestone are reasonably closely grouped, and show, on average, steeper inclinations (≈ −45°, Figs 9a and b) than the Mjøsa limestone HB overprints (≈ −35°, Fig. 9c). The latter is similar to directional data (Figs 9d and e) from the Upper Carboniferous-Permian Oslo Graben lavas (274–294 Ma) (van Everdingen 1960). Hence, the early Triassic age (≈243 Ma) obtained for the Lunner dykes is reflected by marginally steeper palaeomagnetic inclinations (Fig. 9). Given the complicated Bøverbru palaeomagnetic signature (see below), we base our new early Triassic palaeomagnetic pole (243 Ma) entirely on the Lunner dykes and contacts (Fig. 10, Table 6). Based on the Lunner data we calculate a palaeolatitude of 25°N for the Oslo region at ≈243 Ma; this fits well with lithofacies indicators, and as an example, the

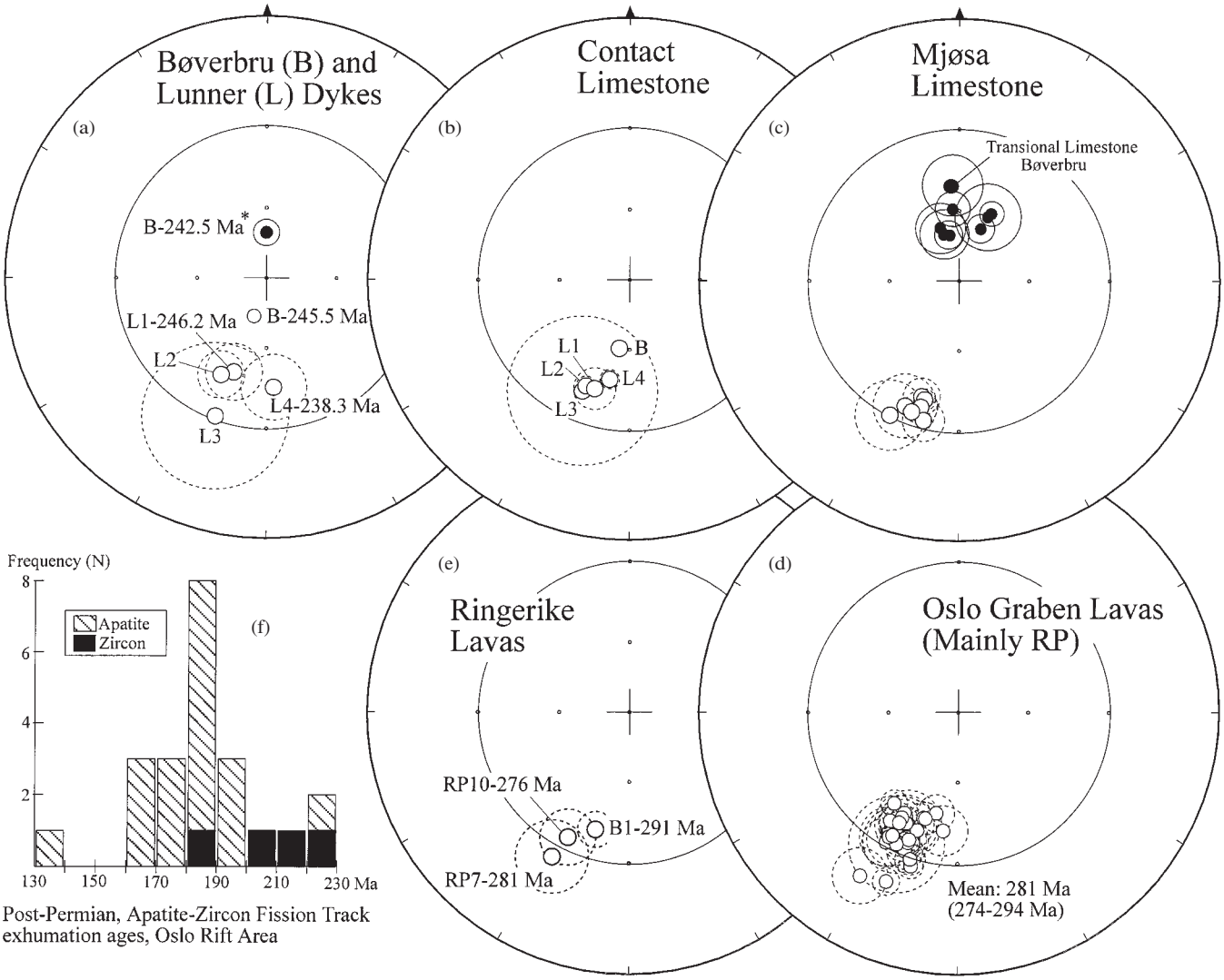

Figure 9. Site-mean directions from Bøverbru–Lunner dykes (a), contact/baked limestone (b), and the regional Mjøsa Limestone (c). Also shown are mean directions from the Ringerike Lavas, 276–291 Ma (e: after Douglass 1989), and site-mean directions from the Oslo Graben Lavas, 274–294 Ma (d: after van Everdingen 1960). (f) frequency distribution of post-Permian, apatite-zircon fission-track ages, Oslo Rift area (after Rohrmann et al. 1994).

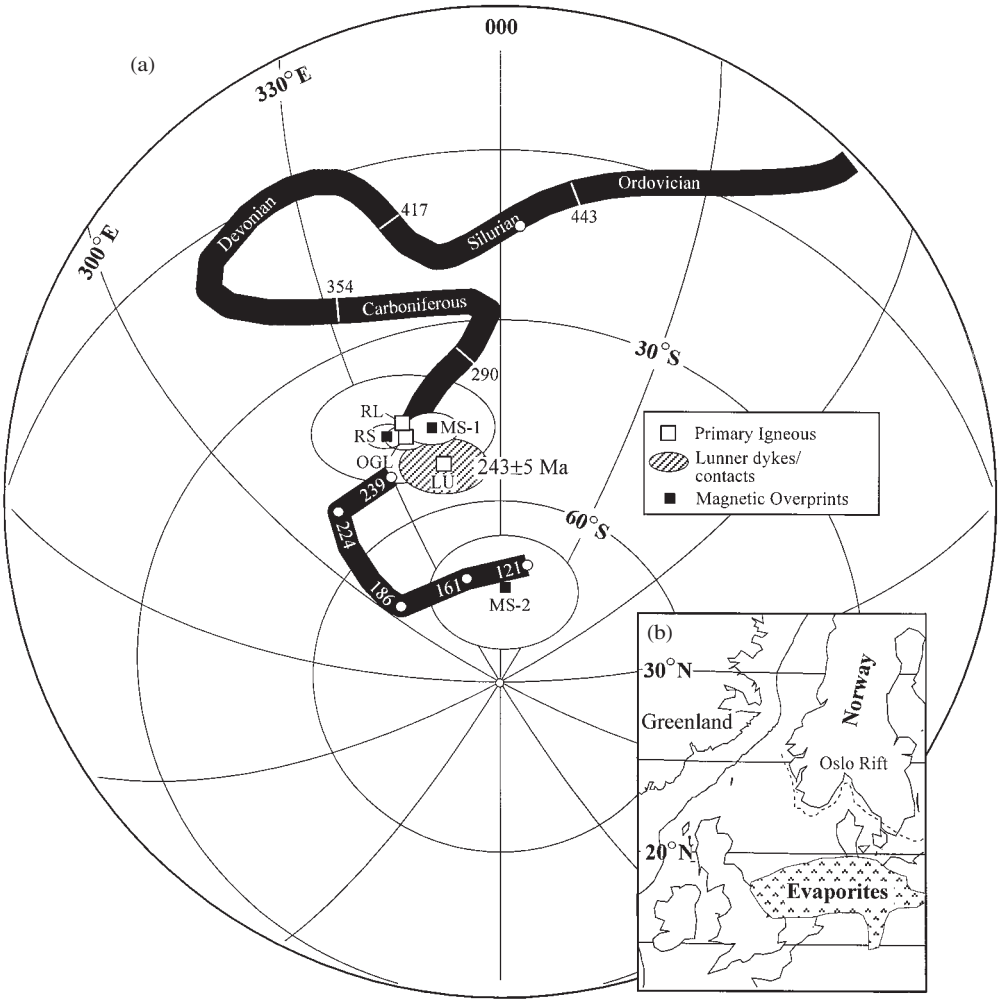

Figure 10. (a) Palaeozoic apparent polar wander path for Baltica (Torsvik et al. 1996) extended with that of stable Europe (Van der Voo 1993) from early Triassic times. Poles (Table 6) derived from the present study (MS-1: Mjøsa Limestone HB; MS-2: Mjøsa Limestone LB; LU: Lunner dykes and contacts) are plotted along with 'primary' igneous poles from the Oslo igneous province [RL: Ringerike Lavas (large errors since only three sites) and OGL: Oslo Graben Lavas]. Also included is a palaeomagnetic overprint pole from the Ringerike Sandstone (RS). Note the concordance between MS-1 and RS (magnetic overprints), and OGL and RL, which suggests regional remagnetization between 294 and 274 Ma (see text). (b) Early Triassic (243 Ma) reconstruction using the mean Lunner pole. Equal-area projections.

main outcrop of Zechstein evaporates (Ziegler 1990) plots between 17 and 20°N in our palaeomagnetically controlled reconstruction (Fig. 10b).

Complex Bøverbru dyke remagnetization

The reverse direction for the Bøverbru dyke has a somewhat steeper inclination than that for the Lunner dykes. A partial positive contact test may indicate that the dyke was intruded in a reverse polarity field, but we also show that the interior parts of the dyke record a normal polarity field. The unusual antipodal magnetic characteristic for the Bøverbru dyke is probably the result of remagnetization of the interior parts of the dyke.

The normal polarity Bøverbru inclinations in the dyke centre interior resemble LB components from the dyke margin and the regional LB components in the Mjøsa Limestone (see below) and suggest that a Jurassic, or younger, thermochemical or viscous overprint strongly affected the coarse-grained interior parts of the dyke and is further observed as a LB component in marginal samples. We propose the following series of events as an explanation for the observed magnetic signature of the dyke:

(1) an original, 243 Ma reverse magnetization during intrusion crystallization of the dyke that was preserved in the dyke chilled margin and limestone baked contact, followed by

(2) a Jurassic, or younger, magnetic resetting that preferentially affected the coarse-grained and less stable dyke centre.

However, it is also possible that the partial positive contact test may be an artefact of post-dyke fluid influx along the dyke–limestone contact, which is evident via mineralized veins and fractures and secondary alteration of the host limestone. Low-temperature alteration/maghemitization, relating to fluids, is recognized throughout the dyke (Figs 4c–d), and this may have led to complete remagnetization of the dyke and the contact limestone in a reverse field direction. This maghemitization process enhanced magnetic stability differences, as marginal grains were effectively subdivided by shrinkage cracks

while interior grains retained larger (PSD/MD) magnetite regions which were more easily remagnetized in a younger normal polarity field. Hence, we are inclined to argue that both the margin (reverse) and interior-centre (normal) magnetizations could be of secondary origin.

Mjøsa Limestone

The Cambro-Silurian sequences in the vicinity of the Oslo Rift show a strong Permian magnetic overprint which we relate to extensive magmatism and fluid development during the evolution of the Oslo Rift system. This is exemplified by a negative fold test at the 95 per cent confidence level (i.e. post-fold magnetizations) from the Mjøsa Limestone HB component (Table 2). In situ directions (Figs 9c and d) and hence palaeomagnetic poles are virtually indistinguishable from those of the Oslo Graben/Ringerike Lavas (274–294 Ma; Fig. 10, compare poles OGL: Oslo Graben Lavas, RL: Ringerike Lavas and MS-1: Mjøsa HB component). Similar magnetic overprinting is observed from the Silurian Ringerike Sandstone (Table 6 and Fig. 10, pole RS: Ringerike Sandstone overprint), but primary Silurian directions in these red beds were also recovered above 600 °C (Douglass 1989). Northwards and $\approx$25 km away from the Oslo Rift, but towards the 'Caledonian' front, the Permian overprint in the Mjøsa Limestone vanishes (Perroud et al. 1992; Torsvik et al. in preparation).

LB components from the Mjøsa Limestone also fail a fold test at the 95 per cent confidence level (Table 2), and probably represent Jurassic or younger remagnetization (Fig. 10; pole MS-2). The proposed Jurassic-to-younger resetting of the Mjøsa Limestone and probably also the Bøverbru dyke centre (Figs 9 and 10) can be tied to established tectonic events in the area. Post-rift evolution of the Oslo Rift system, constrained by fission-track thermochronology (Fig. 9f), is interpreted to entail post-rift (i.e. post-Permian) exhumation of 3–4 km; furthermore, the exhumation was differential, but continuous, from the central part to the northwest part of the Oslo Graben during Triassic through to Jurassic time (Rohrmann et al. 1994). The low-temperature (100–300 °C) hydrothermal fluid circulation associated with this exhumation process (Rohrman et al. 1994) would be consistent with the magnetic resetting characteristics we observe in the dykes and the limestones, but were probably neither focused nor intense enough to cause significant resetting of the Ar systematics of the dykes.

CONCLUSIONS

The Lunner and Bøverbru dykes are dated to 243 $\pm$ 5 Ma (2s error) and represent the youngest radiometrically dated dykes in the Oslo Rift area, intruded during the final, curtailed throes of magmatic activity in the graben whilst the Oslo Rift was located at 25°N. The dykes differ in age from the main, Oslo Graben lava pulse (274–294 Ma), which is also reflected by some APW, though small, from Permian to early Triassic times.

The dual-polarity magnetic signature of the Bøverbru dyke, demonstrably of the same intrusion age as those from Lunner, is a complex Mesozoic remagnetization phenomenon.

Extensive Oslo Rift magmatism and fluid development remagnetized the Mjøsa Limestone (HB component) in the Hadeland area at around 274–294 Ma; however, further to the north, and some 25 km away from the main Oslo Rift magmatism, the Permian remagnetization is absent.

The Mjøsa Limestone has also undergone, at least locally, a younger thermo-chemical remagnetization event (LB component), probably of Jurassic or younger age, which is demagnetized at temperatures below 150–300 °C.

ACKNOWLEDGMENTS

We thank Mobil, the Norwegian Research Council, Phillips and Statoil for financial support. ONOFF contribution no. 4.

REFERENCES

Ade-Hall, J.M., Palmer, H.C. & Hubbard, T.P., 1971. The magnetic and opaque petrological response of basalts to regional hydrothermal alteration, Geophys. J. R. astr. Soc., 24, 137–174.

Arnaud, N.O., Brunel, M., Cantagrel, J.M. & Tapponier, P., 1993. High cooling and denudation rates at Kongur Shan, eastern Pamir (Xinjiang, China) revealed by 40Ar/39Ar alkali feldspar thermocronology, Tectonics, 12, 1335–1346.

Bjørlykke, K., 1983. Subsidence and tectonics in Late Precambrian and Palaeozoic sedimentary basins of Southern Norway, Nor. Geol. Unders. Bull., 380, 159–172.

Cebula, G.T., Kunk, M.T., Mehnert, H.N., Naeser, C.W., Obradovich, J.D. & Sutter, J.F., 1986. The Fish Canyon Tuff, a potential standard for the 40Ar-39Ar and fission-track dating methods (abstract), Terra Cognita, 6, 139–140.

Douglass, D.N., 1989. Palaeomagnetics of Ringerike Old Red Sandstone and related rocks, southern Norway: Implications for pre-Carboniferous separation of Baltica and British Terranes, Tectonophysics, 148, 11–27.

Eide, E.A. & Torsvik, T.H., 1996. Paleozoic supercontinental assembly, mantle flushing, and genesis of the Kiaman Superchron, Earth planet. Sci. Lett., 144, 389–402.

Heeremans, M., Larsen, B.T. & Stel, H., 1996. Paleostress reconstruction from kinematic indicators in the Oslo Graben, southern Norway: new constraints on the mode of rifting, Tectonophysics, 266, 55–79.

Maluski, H., 1989. Argon 40-argon 39 dating: Principles and applications to minerals from terrestrial samples, in Nuclear Methods of Dating, pp. 325–352, eds Roth, E. & Poty, B., Kluwer Academic, Hingham, MA.

Neumann, E.-R., 1994. The Oslo Rift: P-T relations and lithospheric structure, Tectonophysics, 240, 159–172.

Neumann, E.-R., Larsen, B.T. & Sundvoll, B., 1985. Compositional variations among gabbroic intrusions in the Oslo Rift, Lithos, 18, 35–59.

Olaussen, S., Larsen, B.T. & Steel, R., 1994. The Upper Carboniferous-Permian Oslo Rift: Basin fill in relation to tectonic development, in Pangea: Global Environments and Resources, Can. Soc. Petrol. Geol. Mem., 17, 175–197.

Opalinski, P.R. & Harland, T.L., 1981. The Middle Ordovician of the Oslo Region, Norway, 29, Stratigraphy of the Mjøsa Limestone in the Toten and Nes-Hamar areas, Nor. Geol. Tidsskr., 61, 59–78.

Perroud, H., Robardet, M. & Bruton, D.L., 1992. Palaeomagnetic constraints upon the palaeogeographic position of the Baltic Shield in the Ordovician, Tectonophysics, 201, 97–120.

Ramberg, I.B., 1976. Gravity interpretation of the Oslo Graben and associated igneous rocks, Nor. Geol. Unders. Bull., 325.

Ramberg, I.B. & Larsen, B.T., 1978. Tectonomagmatic evolution, in The Oslo Paleorift, a Review and Guide to Excursions, eds Dons, J.A, & Larsen, B.T, Nor. Geol. Unders. Bull., 337, 55–73.

Rohrmann, M., Van der Beek, P. & Andriessen, P., 1994. Syn-rift thermal structure and post rift evolution of the Oslo Rift (southeast Norway): New constraints from fission track thermochronology, Earth planet. Sci. Lett., 127, 39–54.

Sundvoll, B. & Larsen, B.T., 1990. Rb-Sr isotope systematics in the magmatic rocks of the Oslo Rift, Nor. Geol. Unders. Bull., 418, 27–46.

Sundvoll, B. & Larsen, B.T., 1993. Rb-Sr and Sm-Nd relationships in dyke and sill intrusion in the Oslo Rift and related areas, Nor. Geol. Unders. Bull., 425, 25–41.

Sundvoll, B. & Larsen, B.T., 1994. Architecture and early evolution of the Oslo Rift, Tectonophysics, 240, 173–189.

Torsvik, T.H. & Eide, E.A., 1998. NGU GEOCHRON: Database and analysis package for Norwegian isotope geochronology, Norwegian Geological Survey, Open file report no. 98.003.

Torsvik, T.H., Smethurst, M.A., Meert, J.G., Van der Voo, R., McKerrow, W.S., Brasier, M.D., Sturt, B.A. & Walderhaug. H.J., 1996. Continental break-up and collision in the Neoproterozoic and Palaeozoic. A Tale of Baltica and Laurentia, Earth Sci. Rev., 40, 229–258.

Van der Voo, R., 1993. Paleomagnetism of the Atlantic, Tethys and Iapetus Oceans, Cambridge University Press, New York.

Van Everdingen, R.O., 1960. Palaeomagnetic analysis of Permian extrusives in the Oslo Region, XVII Skr, Nor. Vidensk. Akad. Oslo, 1, 1–80.

Ziegler, P.A., 1990. Geological Atlas of Western and Central Europe 1990, Shell, Mijdrecht, the Netherlands.